ISSN 1064-2269, Journal of Communications Technology and Electronics, 2016, Vol. 61, No. 6, pp. 607–613. © Pleiades Publishing, Inc., 2016.
Original Russian Text © A.P. Anyutin, I.P. Korshunov, A.D. Shatrov, 2016, published in Radiotekhnika i Elektronika, 2016, Vol. 61, No. 6, pp. 568–574.

ELECTRODYNAMICS AND WAVE PROPAGATION

Quasi-Static Plasmon Resonances in a Graphene Ribbon in the Infrared Range

A. P. Anyutin, I. P. Korshunov, and A. D. Shatrov

Kotel'nikov Institute of Radio Engineering and Electronics (Fryazino Branch), Russian Academy of Sciences, pl. Vvedenskogo 1, Fryazino, Moscow oblast, 141190 Russia

e-mail: anioutine@mail.ru, korip@ms.ire.rssi.ru

Received September 18, 2015

Abstract—The 2D problem of diffraction of a plane electromagnetic wave diffraction by a graphene ribbon is considered for the case of the *TM* polarization. Quasi-static plasmon resonanses are investigated with the use of rigorous numerical methods. The surface currents and scattering and absorption cross-sections are calculated. It is shown that, owing to the high Q-factor, multipole plasmon resonances appear not only in the near field but also in the far field.

DOI: 10.1134/S1064226916060024

INTRODUCTION

The interest to the properties of surface plasmon polaritons is first of all due to the high spatial field localization, which makes possible to use these polaritons in the subwave and near-pole optics. Silver and golden nanowires are widely used as sensors [1]. Plasmon resonances in them are realized in the ultraviolet part of the spectrum [1]. The use of silver nanotubes makes possible to shift the frequencies of plasmon resonances into the visible part of the light spectrum [2, 3].

New material graphene, which was recently discovered, is a monoatomic graphite layer, in which carbon atoms form a 2D crystalline lattice with the distance between neighboring atoms 0.142 nm [4]. Graphene exhibits unique electron-optical properties in the wide frequency band stretching from the light to terahertz range. The electrodynamic characteristics of structures with graphene elements may change under the influence of an exterior electric field [5]. Therefore, various devices of nanodimensional electronics—sensors, modulators, switches, and filters—can be produced on the basis of graphene [6, 7].

A great number of works are devoted to scattering of electromagnetic radiation by graphene objects of different geometry (for example, see [7] and the bibliography cited there). In works [8, 9], plasmon resonances appearing when a terahertz plane electromagnetic wave is diffracted by a graphene ribbon are numerically investigated. In this work, the resonance properties of a graphene ribbon in the infrared range are studied.

1. FORMULATION OF THE PROBLEM AND THE METHOD OF SOLUTION

The problem of the plane wave diffraction by a graphene ribbon is considered (Fig. 1). The plane wave propagates in the free space along the direction of the unit vector $(\cos\varphi_0, \sin\varphi_0, 0)$ and is characterized by the following components of the electromagnetic field:

$$\begin{aligned} H_z^0 &= \exp(-ikx\cos\varphi_0 - iky\sin\varphi_0), \\ E_x^0 &= -\eta\sin\varphi_0\exp(-ikx\cos\varphi_0 - iky\sin\varphi_0), \\ E_y^0 &= \eta\cos\varphi_0\exp(-ikx\cos\varphi_0 - iky\sin\varphi_0). \end{aligned} \quad (1)$$

The ribbon of the width $2a$ is located in the plane $y = 0$ and is infinite along the z axis. The dependence on

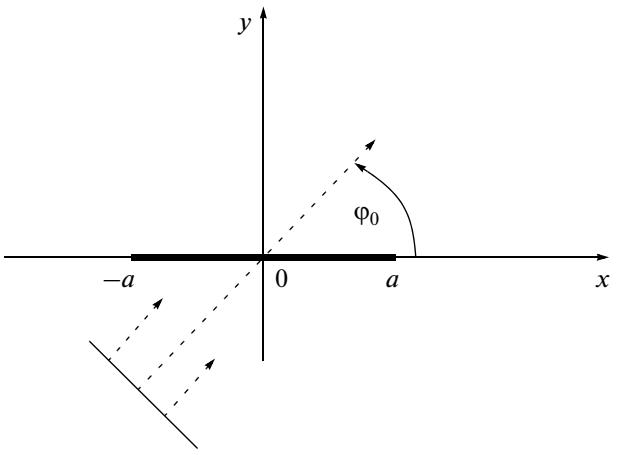

Fig. 1. Geometry of the problem.

time is chosen in the form $\exp(i\omega t)$, where $\omega = kc$, $k = 2\pi/\lambda$, c is the light speed in vacuum, λ is the wavelength, and $\eta = \sqrt{\mu_0/\varepsilon_0} = 120\pi\ \Omega$ is the wave impedance of free space.

It is more suitable to investigate the formulated problem with the use of the z component of the magnetic field $U(x,y) = H_z(x,y)$. The boundary problem for function $U(x,y)$ is scalar.

Complete field $U(x,y)$ satisfies the Helmholtz equation

$$\frac{\partial^2 U}{\partial x^2} + \frac{\partial^2 U}{\partial y^2} + k^2 U = 0. \quad (2)$$

The components of the electric field can be expressed in terms of function $U(x,y)$:

$$E_x = \frac{\eta}{ik}\frac{\partial U}{\partial y}, \quad E_y = -\frac{\eta}{ik}\frac{\partial U}{\partial x}. \quad (3)$$

The boundary conditions on a graphene ribbon have the form [10]

$$\begin{aligned} E_x(x,+0) &= E_x(x,-0), \quad |x| < a, \\ H_z(x,+0) - H_z(x,-0) &= \sigma E_x(x,0), \quad |x| < a, \end{aligned} \quad (4)$$

where σ is the surface conductivity of graphene. For function $U(x,y)$, these conditions have the form

$$\begin{aligned} \frac{\partial U}{\partial y}(x,+0) &= \frac{\partial U}{\partial y}(x,-0), \quad |x| < a, \\ U(x,+0) - U(x,-0) &= \frac{\eta\sigma}{ik}\frac{\partial U}{\partial y}(x,0), \quad |x| < a. \end{aligned} \quad (5)$$

The complete field consists of the incident (U^0) and scattered (U^s) fields

$$U = U^0 + U^s. \quad (6)$$

The incident field is specified by the function

$$U^0 = \exp(-ikx\cos\varphi_0 - iky\sin\varphi_0). \quad (7)$$

In the cylinder coordinate systems ($x = r\cos\varphi$, $y = r\sin\varphi$), the scattered field must satisfy the radiation condition in the far zone

$$U^s \sim \Phi(\varphi)\sqrt{\frac{2}{\pi kr}}\exp\left(-ikr + i\frac{\pi}{4}\right), \quad kr \to \infty, \quad (8)$$

where $\Phi(\varphi)$ is the scattering pattern.

The boundary problem consisting of Eq. (2), boundary conditions (5), and radiation condition (8) can be reduced by standard methods to the integro-differential equation for the function

$$g(x) = U(x,+0) - U(x,-0), \quad |x| < a, \quad (9)$$

which has the sense of the surface current on the ribbon. This equation has the form

$$\begin{aligned} &\frac{1}{4k}\left(\frac{d^2}{dx^2} + k^2\right)\int_{-a}^{a} H_0^{(2)}(k|x-x'|)g(x')dx' \\ &+ \frac{1}{\eta\sigma}g(x) = \frac{1}{ik}\frac{\partial U^0}{\partial y}(x,0), \quad |x| < a, \end{aligned} \quad (10)$$

where $H_0^{(2)}$ is the Hankel function. Equation (10) can be obtained, for example, by the method applied in work [11] for the investigation of the problem of diffraction by an anisotropically conducting ribbon. A solution to Eq. (10) should be looked for in the class of functions equating to zero at the ends of the interval $(-a,a)$:

$$g(-a) = g(a) = 0. \quad (11)$$

This condition provides for the convergence of the integral $\iint|\mathbf{E}|^2 dxdy$ near the ribbon edges (the Meixner condition [12]).

The scattering pattern is expressed in terms of the current according the formulas

$$\Phi(\varphi) = \frac{k}{4}\sin\varphi\int_{-a}^{a} g(x)\exp(ikx\cos\varphi)dx. \quad (12)$$

Scattering and absorption cross sections σ_s and σ_a are determined according the expressions

$$\sigma_s = \frac{2}{\pi k}\int_0^{2\pi}|\Phi(\varphi)|^2 d\varphi, \quad (13)$$

$$\sigma_a = \mathrm{Re}\left(\frac{1}{\eta\sigma}\right)\int_{-a}^{a}|g(x)|^2 dx. \quad (14)$$

According to the optical theorem, we have

$$k\sigma_s + k\sigma_a = -4\,\mathrm{Re}[\Phi(\varphi_0)]. \quad (15)$$

The numerical solution of integro-differential equation (10) is obtained on the basis of the method of continued boundary conditions [13, 14]. The accuracy of the obtained solution is controlled by the fulfillment of condition (15) of the optical theorem.

2. NUMERICAL RESULTS

The surface conductivity of graphene is calculated according to the Kubo formula [10, 15]

$$\sigma = \frac{-2ie^2 k_B T}{\pi\hbar(\hbar\omega - i\Gamma)}\ln\left[2\cosh\left(\frac{\mu}{2k_B T}\right)\right] + \frac{e^2}{4\hbar}\left(\frac{1}{2} + \frac{1}{\pi}\arctan\left(\frac{\hbar\omega - 2\mu}{2k_B T}\right) + \frac{i}{2\pi}\ln\frac{(\hbar\omega + 2\mu)^2}{(\hbar\omega - 2\mu)^2 + (2k_B T)^2}\right), \quad (16)$$

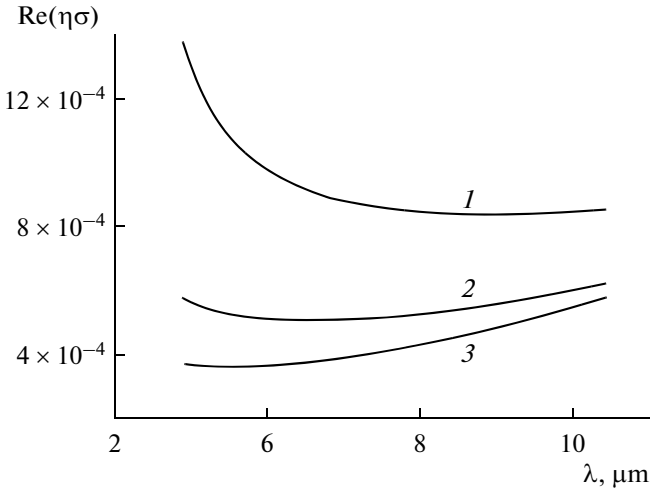

Fig. 2. Dependence of the real part of the surface conductivity of graphene on the wavelength when $T = 300$ K and $\Gamma = 10^{-4}$ eV. Curves *1*, *2*, and *3* correspond to $\mu = 0.3$, 0.5, and 0.7 eV.

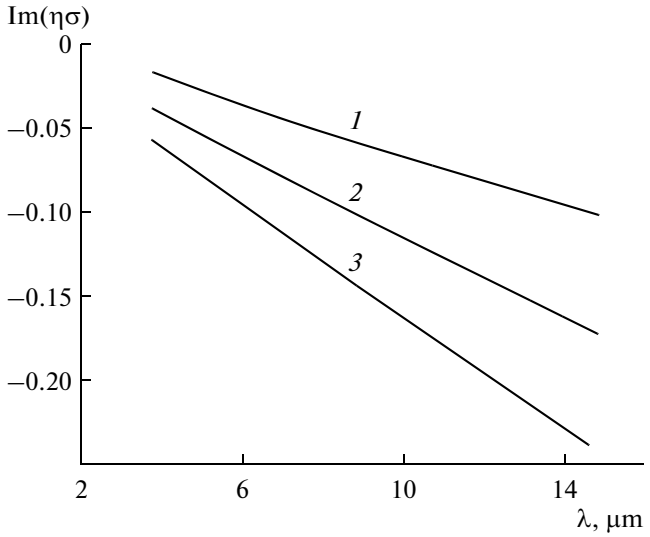

Fig. 3. Dependence of the imaginary part of the surface conductivity of graphene on the wavelength when $T = 300$ K and $\Gamma = 10^{-4}$ eV. Curves *1, 2,* and *3* correspond to $\mu = 0.3$, 0.5, and 0.7 eV.

where e is the electron charge, $\hbar$ is the Planck constant, k_B is the Boltzmann constant, μ is the chemical potential, Γ is the relaxation energy of charge carriers, and T is the graphene temperature.

It is accepted to express energy quantities $\hbar\omega$, k_BT, μ, and Γ in electron-volts. The relationship

$$\hbar\omega \text{ (eV)} = 1.24/\lambda \text{ (μm)} \tag{17}$$

is valid for the photon energy and wavelength. The following values of physical constants are used:

$$k_B = 8.6\times10^{-5} \text{ (eV/K)}, \frac{\eta e^2}{4\pi\hbar} = \frac{1}{137}. \tag{18}$$

In the scientific literature, relaxation time τ, Γ, is often used instead of $\Gamma = \hbar/\tau$.

The dependence of the real and imaginary pats of the dimensionless quantity $\eta\sigma$ on the wavelength is illustrated in Figs. 2 and 3 for the room temperature $T = 300$ K and the parameters typical for graphene. Note that the conductivity of graphene depends on chemical potential μ that can be changed by the applied external electric field. It is seen that, in the considered range of wavelengths, the inequalities

$$\mathrm{Re}(\eta\sigma) \ll -\mathrm{Im}(\eta\sigma) \ll 1 \tag{19}$$

are true.

The surface wave [6]

$$U(x,y) = \begin{cases}\exp(-wy - i\beta x), & y > 0,\\ -\exp(wy - i\beta x), & y < 0,\end{cases} \tag{20}$$

where

$$w = -\frac{2ik}{\eta\sigma} = w' - iw'', \quad \beta = \sqrt{k^2 + w^2} = \beta' - i\beta'' \tag{21}$$

can propagate along a graphene film of infinite dimensions.

Field (20) satisfies Helmholtz equation (2) and boundary conditions (5) in infinite interval $-\infty < x < \infty$.

Formulas (19) and (20) necessitate the inequalities $w' \gg k$ and $\beta' \gg k$, which mean the subwave y localization of the field and oscillations along the x coordinate that are frequent on the wavelength λ scale. Just these properties of the surface wave make possible the existence of plasmon resonances in a ribbon that is narrow as compared to wavelength λ. The resonances appear owing to the surface wave rereflections from the ribbon edges [8, 9].

In all of the calculations, it is supposed that $a = 0.13$ μm and $T = 300$ K. Figure 4 shows the frequency characteristics of absorption cross-sections σ_a for the slide angles $\varphi_0 = \pi/2$ and $\pi/6$ (curves *1* and *2*). It is seen that, in the considered frequency band, curve *1*, which corresponds to the normal incidence, contains four resonance peaks. In the case of the oblique incidence, three additional resonances appear (curve *2*).

Figure 5 shows the distributions of normalized absolute value $|g(x)|$ of the current at the three lower resonance frequencies. These distributions look like standing oscillations. The resonances $ka \approx 0.074$ and 0.14 correspond to wave fields $U(x,y)$ that are even with respect to coordinate x, and resonance $ka \approx 0.11$ correspond to the odd wave fields.

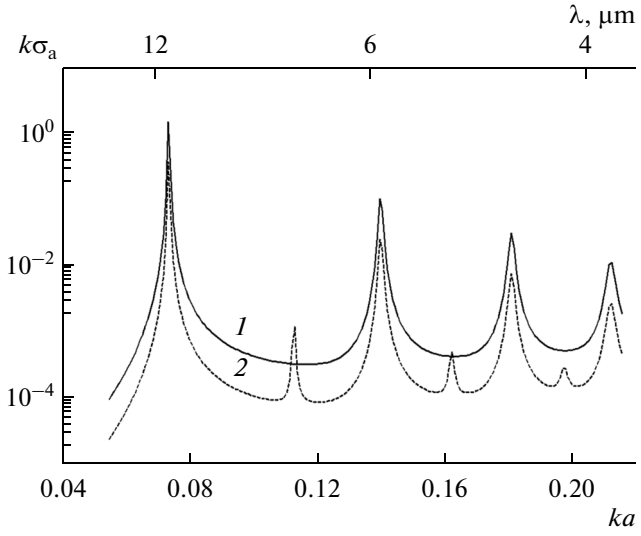

Fig. 4. Frequency dependence of the absorption cross-section of the graphene ribbon when $\Gamma = 10^{-4}$ eV and $\mu = 0.5$ eV. Curves *1* and *2* correspond to $\varphi_0 = \pi/2$ and $\pi/6$.

The charge conservation law makes it possible to express surface charge density $\rho(x)$ in terms of current $g(x)$:

$$\rho(x) = -\frac{1}{i\omega}\frac{dg(x)}{dx}. \qquad (22)$$

It follows from Fig. 5 and formula (22) that, in the case of the dipole resonance ($ka \approx 0.074$), the opposite charges are concentrated near the ribbon edges, and the charge distribution of resonances of the higher orders is described by an alternating function with a large number of oscillations.

Figure 6 shows scattering cross section σ_s for $\varphi_0 = \pi/2$ and $\pi/6$. The comparison of Figs. 4 and 6 shows that the absorption and scattering spectra are substantially different. First, function σ_s has no odd resonances. Second, near higher even resonances, function σ_s has deep dips, which mean that the effect of the ribbon being imperceptible takes place in a narrow frequency band. Formulas (12) and (13) imply that in the quasi-static approximation ($ka \ll 1$), the scattering cross-section is zero when the current on the ribbon satisfies the condition

$$\int_{-a}^{a} g(x)dx = 0. \qquad (23)$$

As a result, the interference suppression of the field develops in the far zone. Figure 7 shows the distribution of absolute value $|g(x)|$ of the current at the frequency of the dip of function σ_s (curve *1*). It is seen that function $g(x)$ approximately satisfies condition (23).

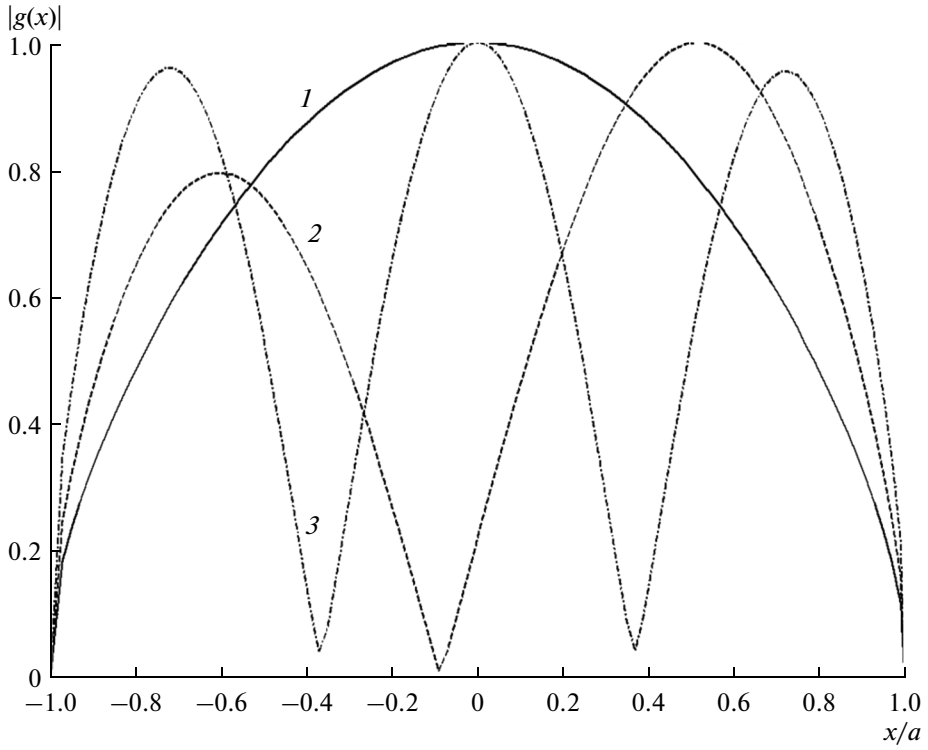

Fig. 5. Normalized distribution of the absolute value of the surface current on the graphene ribbon when $\Gamma = 10^{-4}$ eV, $\mu = 0.5$ eV, and $\varphi_0 = \pi/6$. Curves *1*, *2*, and *3* correspond to the resonance frequencies $ka = 0.074$, 0.11, and 0.14.

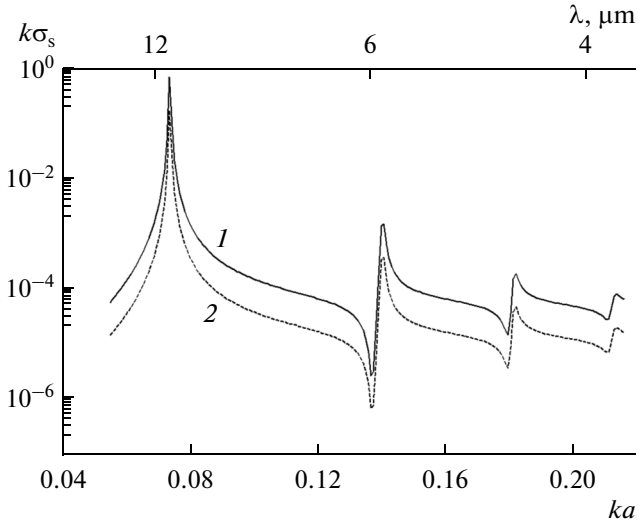

Fig. 6. Frequency dependence of the scattering cross-section of the graphene ribbon when $\Gamma = 10^{-4}$ eV and $\mu = 0.5$ eV. Curves *1* and *2* correspond to $\varphi_0 = \pi/2$ and $\pi/6$.

We discuss in more detail the influence of angle φ_0 on the spectral characteristics of the field. In the quasi-static approximation ($ka \ll 1$), the right-hand part of Eq. (10) can be approximated by the expression

$$-\sin\varphi_0(1 - ikx\cos\varphi_0), \quad |x| < a. \tag{24}$$

The first and second summands in (24) are responsible for the excitation of the even and odd parts of the wave field. Note that the second summand is substantially smaller than the first one and is zero when the plane wave is normally incident ($\varphi_0 = \pi/2$). Therefore, the odd resonances are not excited in the case of the normal incidence, and, in the case of the oblique incidence, they are less expressed than the even resonances (see Fig. 4). It is obvious that condition (23) is automatically fulfilled for odd oscillations. Therefore, function σ_s has no resonance peaks at the corresponding frequencies (see Fig. 6).

Formula (14) implies that the absorbed power is minimal if

$$\int_{-a}^{a} |g(x)|^2\, dx = \min. \tag{25}$$

Figure 7 also shows the current distribution at the frequency $ka = 0.11$, which corresponds to the minimum of the absorbed power (curve *2*). Note that the amplitude of this current is three times less than the current amplitude on curve *1*. However, when $ka = 0.11$, the scattered power is larger by almost two orders of magnitude than the power scattered at the frequency of the dip at $ka = 0.137$. The result, which is unexpected at the first sight, can be explained by the fact that the current distribution at $ka = 0.11$ does not satisfy condition (23) of the far field dip.

Let us investigate the influence of relaxation energy Γ on the properties of plasmon resonances. The heat loss grows with parameter Γ. Figures 8 and 9, respectively, show the spectra of absorbed and scattered

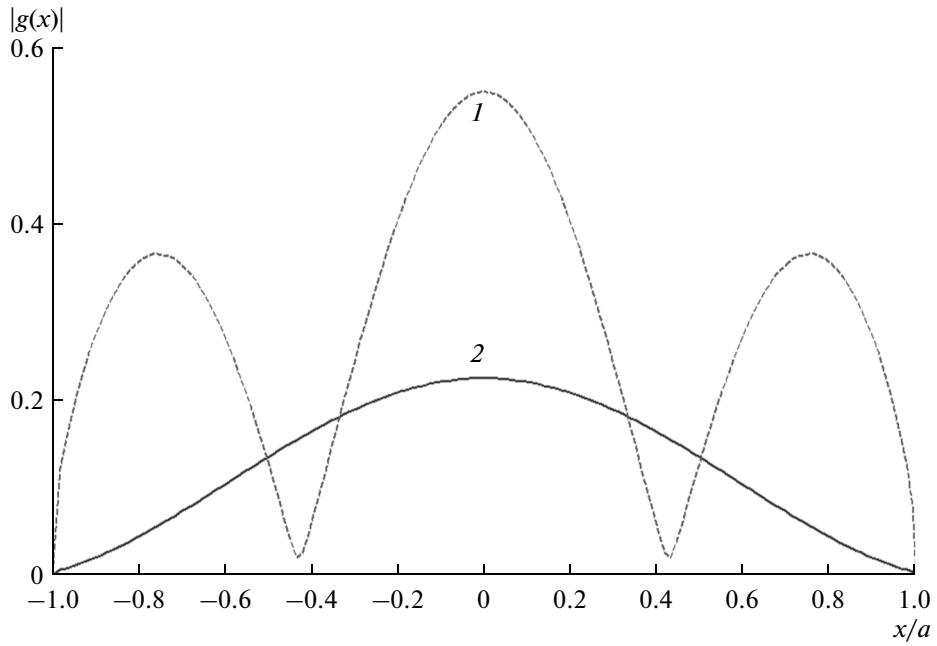

Fig. 7. Distribution of the absolute value of the surface current on the graphene ribbon when $\Gamma = 10^{-4}$ eV, $\mu = 0.5$ eV, and $\varphi_0 = \pi/2$. Curves *1* and *2* correspond to the frequencies $ka = 0.137$ and 0.11.

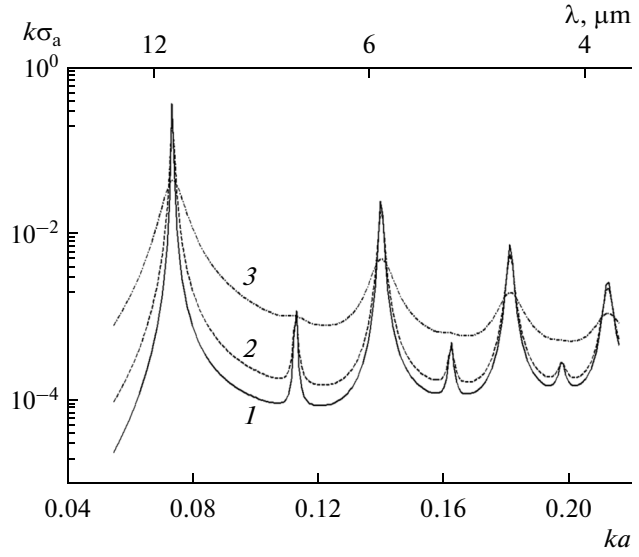

Fig. 8. Frequency dependence of the absorption cross-section of the graphene ribbon when $\mu = 0.5$ eV and $\varphi_0 = \pi/4$. Curves *1*, *2*, and *3* correspond to $\Gamma = 10^{-4}$, 10^{-3}, and 10^{-2} eV.

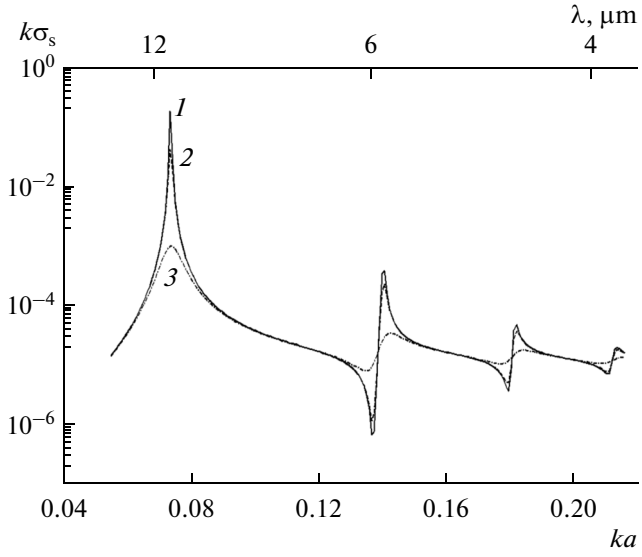

Fig. 9. Frequency dependence of the scattering cross-section of the graphene ribbon when $\mu = 0.5$ eV and $\varphi_0 = \pi/4$. Curves *1*, *2*, and *3* correspond to $\Gamma = 10^{-4}$, 10^{-3}, and 10^{-2} eV.

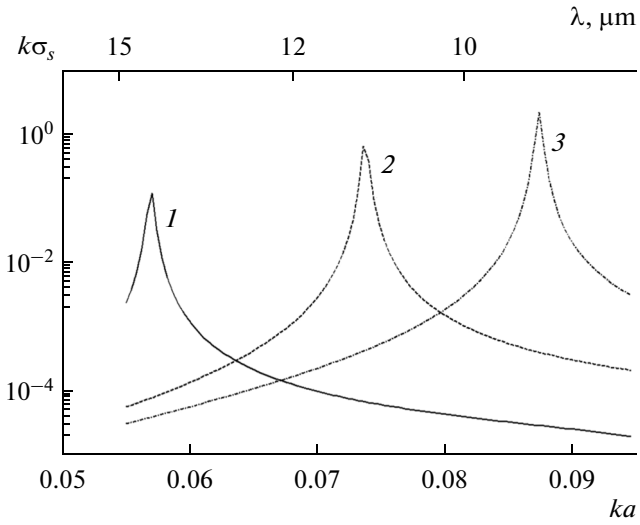

Fig. 10. Frequency dependence of the scattering cross-section of the graphene ribbon when $\Gamma = 10^{-4}$ eV and $\varphi_0 = \pi/2$. Curves *1*, *2*, and *3* correspond to $\mu = 0.3$, 0.5, and 0.7 eV.

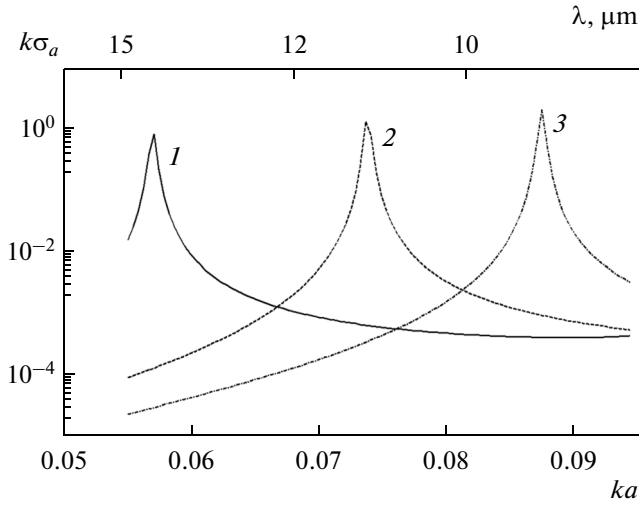

Fig. 11. Frequency dependence of the absorption cross-section of the graphene ribbon when $\Gamma = 10^{-4}$ eV and $\varphi_0 = \pi/2$. Curves *1*, *2*, and *3* correspond to $\mu = 0.3$, 0.5, and 0.7 eV.

power when $\Gamma = 10^{-4}$, 10^{-3}, and 10^{-2} eV. It is seen that, when $\Gamma = 10^{-2}$ eV, the odd resonance disappear in the absorption spectrum as well. Note that, in contrast to a silver cylinder [16], in the graphene ribbon, multipose plasmon resonances become apparent in the far field as well (see Fig. 9) owing to their high Q-factor.

Formulas (12) implies that, for the considered case of narrow ribbons ($ka \ll 1$), the scattering patterns at all frequencies can be approximated by the equation $\Phi \sim A \sin\varphi$. Thus, plasmon resonances become apparent only when amplitude A grows. Note that, in a cylinder, multipole resonances of different orders are characterized by different scattering diagrams $\cos(m\varphi)$ [16].

The position of resonances on curves $\sigma_s(\lambda)$ and $\sigma_a(\lambda)$ can be controlled by the change of chemical potential μ. The influence of the chemical potential on the scattering and absorbing properties of the ribbon in the neighborhood of the dipole resonance is illustrated in Figs. 10 and 11, respectively.

CONCLUSIONS

The resonance effects observed when a plane wave is diffracted by a graphene ribbon were numerically investigated. The influence of the energy of relaxation and the chemical potential of graphene on the absorbing and scattering properties of the ribbon in the infrared wavelength range was considered. It was shown that the absorption and scattering spectra were principally different. It was found that, near even higher resonances, the spectral scattering characteristic had deep dips resulting in the effect of the ribbon obscurity.

ACKNOWLEDGMENTS

This study was supported in part by the Russian Foundation for Basic Research, project no. 16-02-00247-a.

REFERENCES

1. V. V. Klimov, *Nanoplazmonika* (Fizmatlit, Moscow, 2009) [in Russian].
2. E. A. Velichko and A. I. Nosich, Opt. Lett. **38**, 4978 (2013).
3. A. P. Anyutin, I. P. Korshunov, and A. D. Shatrov, J. Commun. Technol. Electron. **60**, 952 (2015).
4. A. K. Geim and K. S. Novoselov, Nature Mater. **6** (3), 183 (2007).
5. L. Ju, B. Geng, J. Horng, et al., Nature Nanotechnol. **6**, 630 (2011).
6. A. Vakil and N. Engheta, Science **332**, 1291 (2011).
7. F. J. de Abajo, ACS Photonics **1** (1), 135 (2014).
8. O. V. Shapoval, J. S. Gomez-Diaz, J. Perruisseau-Carrier, et al., IEEE Trans. Terahertz Sci. Technol. **3**, 666 (2013).
9. M. V. Balaban, O. V. Shapoval, and A. I. Nosich, J. Opt. **15**, 114007 (2013).
10. L. A. Fal'kovskii, Usp. Fiz. Nauk **178**, 923 (2008).
11. P. A. Malyshkin and A. D. Shatrov, J. Commun. Technol. Electron. **44**, 744 (1999).
12. R. B. Vaganov and B. Z. Katsenelenbaum, *Fundamentals of the Diffraction Theory* (Nauka, Moscow, 1982) [in Russian].
13. A. G. Kyurkchan and A. P. Anyutin, Dokl. Math. **66**, 132 (2002).
14. A. P. Anyutin and A. G. Kyurkchan, J. Commun. Technol. Electron. **49**, 11 (2004).
15. Y. Francescato, V. Giannini, and S. A. Maier, New J. Phys. **5**, 063020 (2013).
16. A. P. Anyutin, I. P. Korshunov, and A. D. Shatrov, J. Commun. Technol. Electron. **60**, 572 (2015).

Translated by I. Efimova